World Academy of Science, Engineering and Technology
International Journal of Mechanical and Mechatronics Engineering
Vol:6, No:8, 2012

Analysis of Rail Ends under Wheel Contact Loading

Nannan Zong, Manicka Dhanasekar

***Abstract*—**The effect of the discontinuity of the rail ends and the presence of lower modulus insulation material at the gap to the variations of stresses in the insulated rail joint (IRJ) is presented. A three-dimensional wheel – rail contact model in the finite element framework is used for the analysis. It is shown that the maximum stress occurs in the subsurface of the railhead when the wheel contact occurs far away from the rail end and migrates to the railhead surface as the wheel approaches the rail end; under this condition, the interface between the rail ends and the insulation material has suffered significantly increased levels of stress concentration. The ratio of the elastic modulus of the railhead and insulation material is found to alter the levels of stress concentration. Numerical result indicates that a higher elastic modulus insulating material can reduce the stress concentration in the railhead but will generate higher stresses in the insulation material, leading to earlier failure of the insulation material

***Keywords*—**Rail end, material interface, wheel-rail contact, stress, finite element method

I. Introduction

EFFECT of contacting solids with discontinuous structural stiffness or different material properties within the contact region is a problem of great interest in contact mechanics. The presence of such discontinuity can be found in various adhesively jointed structures, such as the insulated rail joint (IRJ). IRJ is a passive system in the railway signaling track circuit. For automated signaling circuitry, it is required to have two length of rails electrically insulated from one another at their rail ends forming a gap, whilst the joint gap capable of allowing safe passage of loaded wheel. However, due to the difference between the stiffness of the insulation material and the rail, the IRJ is subjected to high stress concentration, which induces various failure modes. Higher axle loads and increased throughput reduce the service life of IRJ, which varies from as low as 7% to 35% of the life of the continuously welded rails (CWR).

Fundamental study of geometrical edge effect subjected to loading due to contacting solids is a very complex problem that cannot be solved using closed form analytical methods; in spite of the advent of computer methods, this problem has received only limited attention in the literature. Based on the Boussinesq-Cerruti method for point loading acting on elastic half-space (Tan and Bushan [1]; Li and Berger [2]; Wilner [3]; Chen and Wang [4]; Liu and Hua [5]),

Nannan Zong is with Faculty of Science & Engineering, Queensland University of Technology, Australia. e-mail: roger.zong@qut.edu.au

* Professor Manicka Dhanasekar is in Faculty of Science & Engineering, Queensland University of Technology, Gardens Point Campus, Queensland University of Technology, Brisbane QLD 4000 Australia. (Phone: +61-7-3138-6666; e-mail: m.dhanasekar@qut.edu.au).

Some semi-analytical solutions for 2D and 3D free-traction edge effect problems subjected to prescribed loading have been investigated in (Hetenyi [6]; Keer et al. [7]; Hanson and Keer [8]). All of these techniques unavoidably introduces internal shear and normal stresses at the free-traction surfaces and successive superposition of the solution for the elastic half-space (correction methods) are required to eliminate the internal stresses normal to the free surface, which requires significant computational effort. Recently by (Guilbault et al. [9]; Guilbault [10]), partial correction methods are presented as the efficient analytical correction solution procedure.

The fundamental study as mentioned above was then further applied to the contacting solids problems. Numerical investigation of a wedge contact was performed by Gerber [11], who evaluated a rigid frictionless punch contacting a quarter plane (wedge angle equals to 90°) using Hetenyi's method [6]. Erdogan and Gupta [12] studied frictionless flat punch contacting with a two dimensional wedge at arbitrary angles and discussed the singularity of the contact pressure as a function of wedge angle when contact approaches the wedge apex. The contact pressure close to the vertical free edge has been studied by Hanson and Keer [13] for a frictionless contact of an elastic quarter plane and Keer et al. [14] for a quarter space contact. The contact distribution at the free edge is shown to exhibit different characteristics to those away from the free edge even for simple loading. Bosakov [15] and Guenfoud et al. [16] conducted the analysis of a deformable rectangular plate resting on the surface of an elastic quarter-space close to the vertical free traction edge. They applied Ritz's method to obtain accurate results for the contact pressure, and vertical displacements of an elastic quarter-space.

As for the wheel-rail contact problem in the vicinity of the gap of the IRJ, the interface between the railhead end and the insulation material defines the problematic vertical edge. More importantly, this vertical edge is subjected to unknown traction provided by the insulation material and the analytical or semi-analytical solution are very complex to formulate. Therefore, numerical tools are used for exploring the wheel-rail contact problem. Yan and Fisher [17] used three-dimensional finite element (FE) model to investigate the wheel-rail contact problem, their result indicated that the Hertzian prediction can be applied if the material is assumed to be linear and the geometrical effect can be ignored such as CWR. Chen [18] developed a two-dimensional line contact FE model to simulate the effect of a free-traction rail end on the contact and stress variation. Chen and Kuang [19] proposed a three-dimensional FE model for the study of the effect of the rail ends with insulation material on the contact stress behavior; however, they only considered the situations, where the ratio of the elastic

modulus between the insulation material and rail is below 0.2. Besides, limited information was reported in terms of the stress variation at the gap of the IRJ. Dynamic analysis of the IRJ (Wen et al. [20]; Cai et al. [21]) and material deterioration (Sandström and Ekberg [22]) are also solved using FE modeling.

In this paper, a three-dimensional finite element method is described to investigate the effect of the discontinuity of the elastic modulus between the rail end and the insulation material in the vicinity of the gap of the IRJ. The normalized contact stress and stresses variation are presented and compared with Hertzian prediction and results from Chen [18]. More importantly, the effect of various ratios of the elastic modulus between rail and the insulation material are reported.

II. Wheel-Rail Contact Modeling at IRJ

A. Hertzian contact theory

As the wheel is located far away from IRJ, the contact can be treated as Hertzian contact problem. Under the normal load F at the wheel centre, the contact region is in elliptical shape, with a major semi axis *a* and a minor semi-axis *b*. The contact pressure *P* distribution in this elliptical contact region is defined as:

$$P = P_0\sqrt{1-(\frac{x}{a})^2-(\frac{y}{b})^2} \quad (1)$$

in which P_0 is the maximum contact pressure at initial contact point between the wheel and the rail, and it is expressed as:

$$P_0 = \frac{3F}{2\pi ab} \quad (2)$$

The semi-axis *a* and *b* are along the *x* axis and *y* axis respectively as shown in the coordinate system in Fig. 1. In order to calculate the axes *a* and *b*, the coefficients *m*, *n*, K_1, K_2 and K_3 are defined by Dukkipati (2000) and *a* and *b* is given by:

$$a = m(\frac{3\pi F(K_1+K_2)}{4K_3})^{1/3} \quad (3)$$

$$b = n(\frac{3\pi F(K_1+K_2)}{4K_3})^{1/3} \quad (4)$$

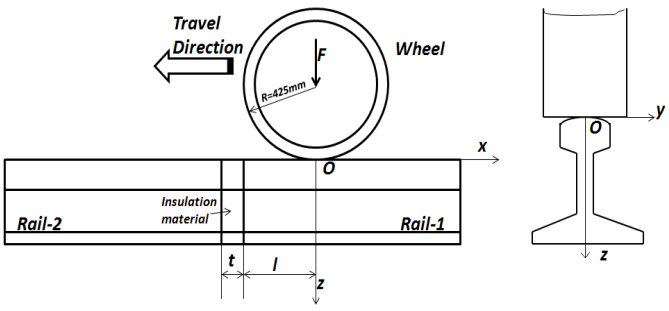

Fig. 1 Wheel-rail contact configuration at IRJ

B. Finite element modeling

In this paper, a three-dimensional finite element model was established to simulate the wheel-rail contact at various proximities to the IRJ. As shown in Fig. 1, a cylindrical shape of wheel subject to normal load *F* was assumed to contact at the centre line of the rail for simplicity. The contact distance *l* is defined as the distance from the initial wheel contact point to the vertical rail end, and the initial wheel-rail contact point is always regarded as the origin of the *xoz* coordinates system. The wheel and the rail have the same elastic material property in terms of Young's modulus E_1=210*GPa* and Poisson's ratio v_1=0.3, while lower elastic modulus E_2=0.2E_1 and same Poisson's ratio v_2=v_1 is applied to the insulation material. *t* denotes the insulation material thickness. Dimensions of the modeled sections of the wheel and rail were chosen to be large enough to limit boundary effect. By allowing for reasonable computational effort, fine mesh with full integration solid element (in ABAQUS, 3D8) was used around the wheel railhead contact region, while coarse mesh with reduced integrated solid element (3D8R) was used in regions away from the contact. In all numerical simulations, the insulation material was assumed to be perfectly bonded with the rail ends. Since the simulation was conducted for different contact distances, the rail model was remeshed at each contact distance l to make sure that fine mesh was placed in the zone of contact. Typical finite element meshes for the wheel-rail contact in the vicinity of the gap of the IRJ is shown in Fig. 2. Definition of contact interaction between the wheel and the rail in ABAQUS is very sensitive to iteration convergence, result accuracy and computational time. The master/slave contact surface method was employed throughout the simulations. The wheel tread surface was defined as master contact surface, while the top surface of IRJ was defined as slave contact surface. The contact surface pair was allowed for finite sliding by defining the friction coefficient between them as μ =0.3. In the static analysis, hard contact was chosen for the contact pressure-over closure relationship in ABAQUS/Standard. The penalty method was used to enforce the contact constraints, which searched for slave node penetrations into the current configuration in all iterations. Contact forces as a function of the penetration distance were applied to the slave nodes to oppose the penetration, while equal and opposite forces acted on the master surface at the penetration point. As the master surface was defined using the element faces, the master surface contact forces were distributed to their nodes.

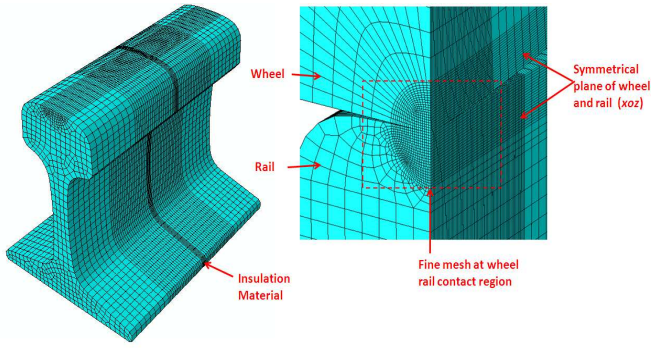

Fig. 2 Finite element mesh

III. Result and Discussion

A. Contact pressure

The variations of the contact pressure between the wheel and the IRJ at different contact distances was discussed in this section. Under the wheel load F=130*KN*, the maximum contact pressure P_0 major semi-axis *a* and minor semi-axis *b* calculated from Hertz formulations is 1381*MPa*, 7.5*mm* and 5.98*mm* respectively. The normalized contact pressure P/P_0 and the normalized coordinates (*x/a* and *y/b*) are presented and compared with the Hertzian prediction as well as Chen [18]. As shown in Fig. 3(*a*) and (*b*), the distribution of the contact pressure obtained from the FE model forms the ellipsoidal shape and matches well with the Hertzian prediction as well as the Chen's result. The maximum difference in terms of the contact pressure, major semi-axis and minor-axis is found to be less than 3% in these two contact distance, i.e. *l/a*=1.60 and 0.96. It indicates that the proposed FE model is capable of predicting accurate contact result, and also proves that the contact variations are not sensitive to the contact distance before the contact extends beyond the rail end, i.e. *l/a*>0.96 and the rail ends effect can be ignored.

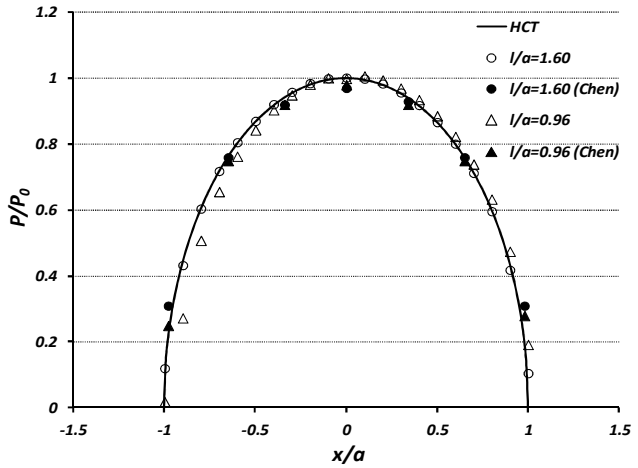

(a)

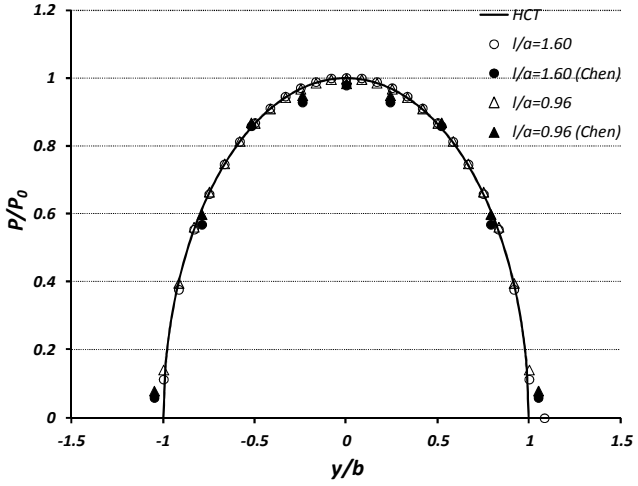

(b)

Fig. 3 Distribution of contact pressure at contact distances: (*a*) *l/a*=1.60; (*b*) *l/a*=0.96

However, when the contact region extends beyond the rail end, i.e. *l/a*=0.32, 0.0 and -0.4 (-0.4 denotes that the wheel is located in the middle of the insulation material between the rail ends), the contact pressure distribution along the *x* axis deviates significantly from the ellipsoidal shape. Fig. 4 illustrates that the contact region is divided into two portions, one between the wheel and the rail and the other between the wheel and the insulation material. Similar to Chen [18], at contact distance *l/a*=0.32, the contact pressure between the wheel and the rail slightly increased, while the contact pressure over the insulation material has dropped below $0.4P_0$. As the wheel further moves and contacts with the other rail end (Rail-2) i.e. *l/a*= 0 and -0.4, the contact pressure exhibits two peak values, with the maximum peak around $1.23P_0$ in *l/a*=0 and $1.17P_0$ in *l/a*=-0.4 respectively. Moreover, a wider contact length was found with the deceasing contact distance *l/a*.

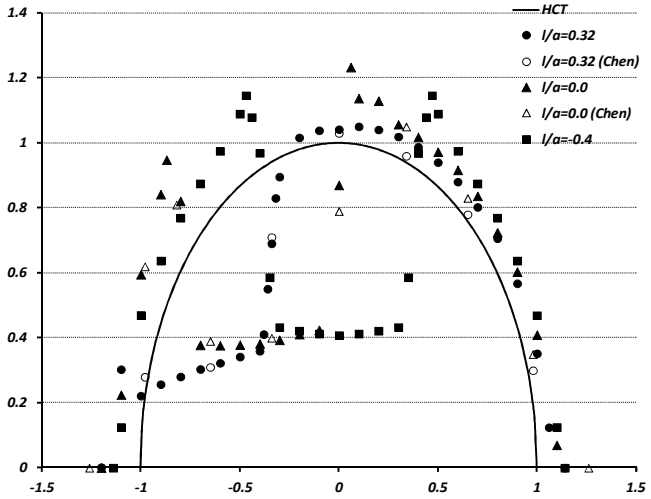

Fig. 4 Distribution of contact stress along x axis at different contact distances

Fig. 5 depicts the contact pressure variations along the *y* axis at different contact distances. Generally, the distribution retains a symmetrical shape at these different contact distances. However, the magnitude reduced significantly at *l/a*=0 and -0.4. The peak contact pressure at *l/a*=0 is reduced to 84% of P_0 in current FE model and 80% of P_0 in Chen [18]. When the wheel was symmetrically located between rail ends, i.e. *l/a*=-0.4, the peak contact pressure further reduced to only around $40\%P_0$. Fig. 6 (*a*) and (*b*) show the three-dimensional contour plots of the contact pressure at *l/a*=0 and -0.4 respectively. The effect of the rail ends is obvious and can be concluded that as the wheel-rail contact is located between the rail ends, the wheel is partially losing contact with the insulation material due to the difference of the elastic modulus between the rail and the insulation material. This results in significant alteration in terms of the magnitude and the distribution of the contact pressure.

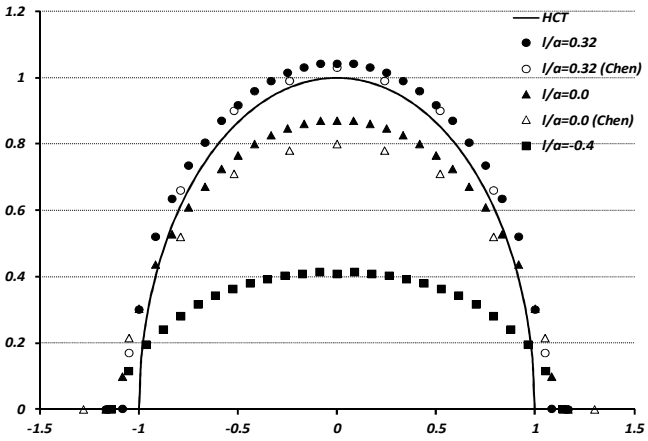

Fig. 5 Distribution of contact stress along y axis at different contact distances

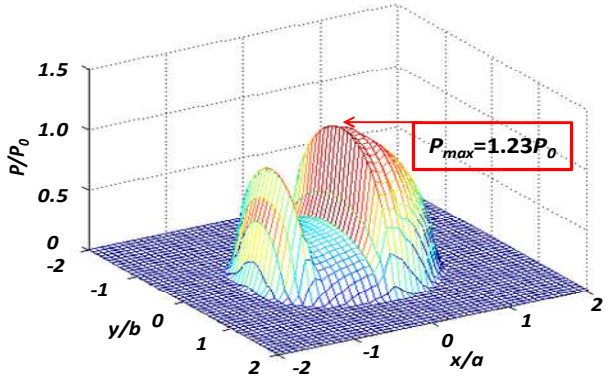

(a)

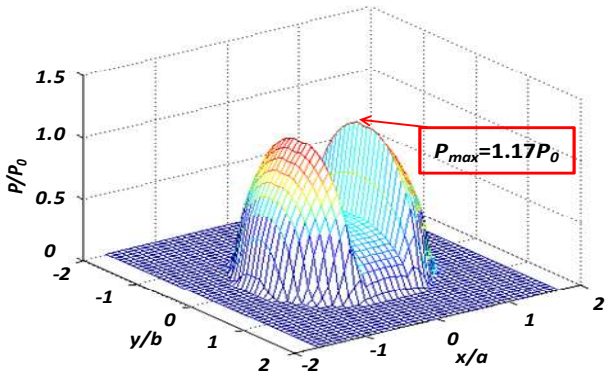

(b)

Fig. 6 Three-dimensional contour plot of contact stress distribution at contact distance: (*a*) *l*/*a*=0.0; (*b*) *l*/*a*=-0.4

B. Stresses variations

The distribution of the normalized maximum shear stress τ_{max}/P_0 along the depth of the symmetrical axis of the rail end surface at various contact distances were presented in Fig. 7. It can be seen that the maximum shear stress is less than $0.1P_0$ in both of the FE model and Chen [18] at the contact distance *l*/*a*=1.60, and the rail ends are experiencing high stress concentration. However, with the wheel moving closer to the rail end, the maximum shear stress has significantly increased especially from the railhead subsurface (*z*/*a*=2) to railhead top surface (*z*/*a*=0). Meanwhile, the peak value is shifting up towards to the rail head top surface. When the wheel is loaded right over the rail end, i.e. *l*/*a*=0, the peak maximum shear stress τ_{max}/P_0 is crowded at the corner of the rail end, valued around $0.54P_0$ for the FE model and $0.5P_0$ for Chen [18]. With the wheel further moving in between the rail ends, i.e. *l*/*a*=-0.4, the peak maximum shear stress topped up to $0.68P_0$. Because the maximum shear stress reflects the failure of the insulation material adhesive, the results from Fig. 7 indicate that the development of high level of shear stress along the interface between the rail end and the insulation material may lead to delamination of the insulation material.

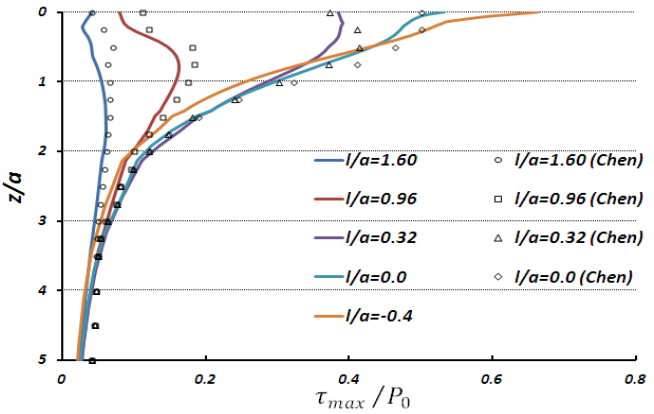

Fig. 7 Maximum shear stress variation along the interface between rail end and insulation material at different contact distances

The von Mises stress is an important factor describing the possibility of the material plastic deformation and material deterioration, the variation of the normalised von Mises stress σ_e/P_0 along the depth of the rail end is presented as shown in Fig. 8. The behaviour of the von Mises stress is similar to the maximum shear stress as presented in Fig. 7. When the wheel approaches the rail end, the peak von Mises stress migrates to the corner of the rail end, with increased values $1.0P_0$ at *l*/*a*=0 and $1.2P_0$ at *l*/*a*=-0.4, they are above yield strength of high yield strength steels used in railhead, whose averaged yield strength σ_y is around 780*MPa* ($0.56P_0$).

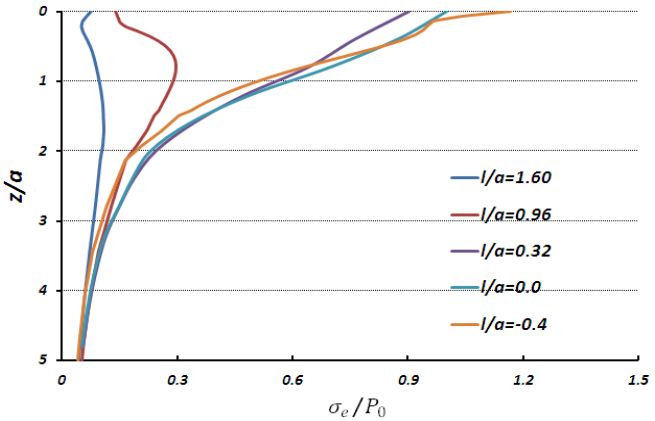

Fig. 8 Von Mises stress variation along the interface between rail end and insulation material at different contact distances

The distribution contours of the von Mises stress in the symmetrical plane of the rails at different contact distances are shown in Fig. 9, which illustrates the stress concentration at the rail end surface. The upper limit of the stress distribution contour is bounded at $0.56P_0$, which represents the yield stress of the rail σ_y. It is found that as the wheel moves close to the rail end i.e. from l/a=1.60 to 0.32, the stress concentration zone above σ_y is shifting towards the rail end and its area is increasing. Moreover, the maximum von Mises stress is migrating from the subsurface to the corner of the rail end, valued $1.6P_0$ at l/a=0.32. As the contact region further extends to the other rail end, i.e. l/a=0 and -0.4, the maximum von Mises stress in both of the rail ends retains at their corners and valued $1.77P_0$ (Rail-1) and $1.47P_0$ (Rail-2) at l/a=0 and around $2.26P_0$ in both of the rail ends at l/a=-0.4. This stress concentration zone crowded at the rail end corner region and its high level of magnitude reveals that the vertical rail end is a serious problem from the wheel-rail contact perspective as it acts as a point of singularity leading to excessive material deterioration.

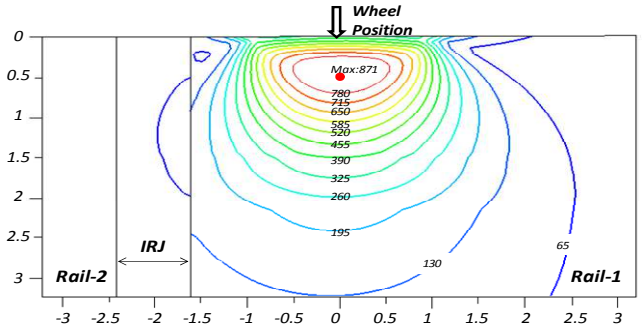

(a)

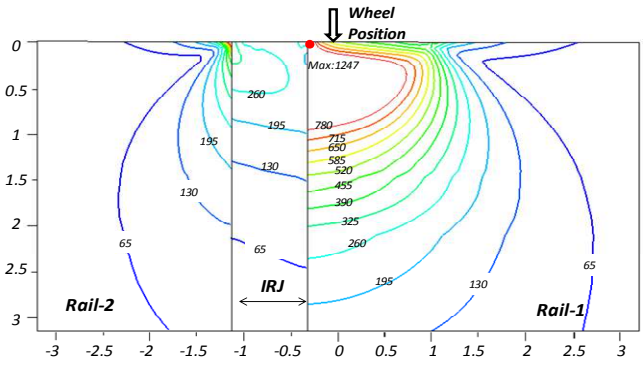

(b)

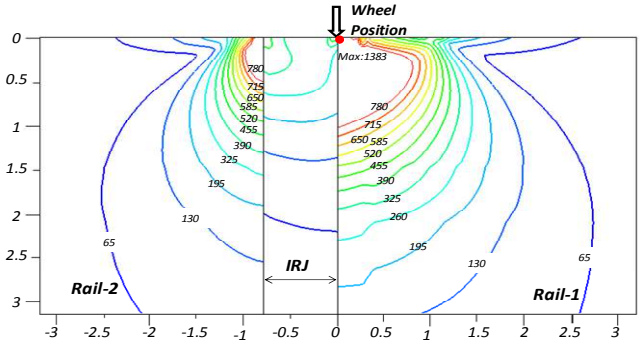

(c)

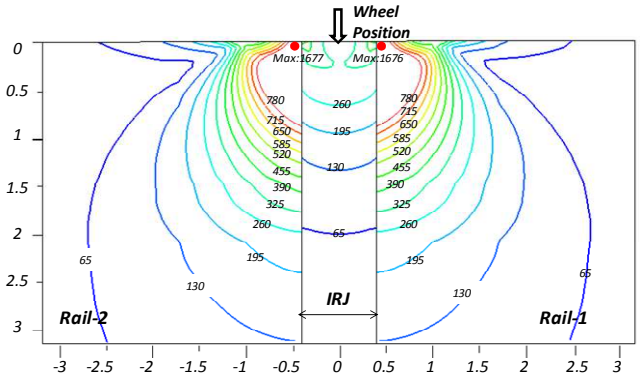

(d)

Fig. 9 Distribution of von Mises stress at IRJ at different contact distances: (*a*) l/a=1.60; (*b*) l/a=0.32; (*c*) l/a=0.0; (*d*) l/a=-0.4

C. Effect of insulation material

The results in the above sections are presented by considering the most commonly used insulation material with the ratio of the elastic modulus E_2/E_1=0.2 between the insulation material and the rail steel. In this section, the effect of different ratios (E_2/E_1) is investigated. Four different ratios were studied and compared, namely E_2/E_1=0.002, 0.2, 0.5 and 0.8.

Fig. 10 and Fig. 11 show the effect of the modulus ratio on the contact pressure along the *x* axis and *y* axis at contact distance l/a=0 and -0.4 respectively. At contact distance l/a=0 and -0.4 as shown in Fig. 10 (a) and (b), the shape of the contact pressure along the *x* axis is affected by the materials of the rail and the insulation material. It is found that the contact pressure on the railhead increase and the insulating material decrease with the reduction in E_2/E_1 from 0.8 to 0.002.

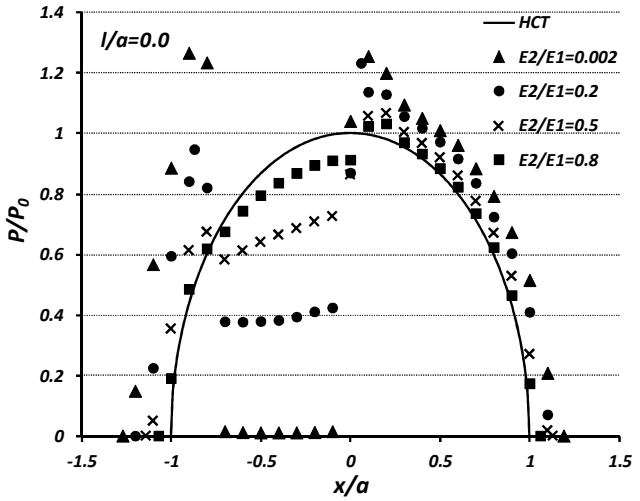

(a)

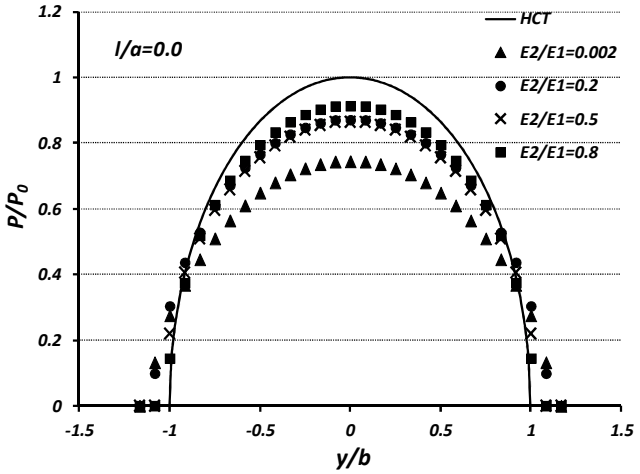

(b)

Fig. 10 Effect of various elastic modulus ratios on the contact stress distribution along: (*a*) *x* axis; (*b*) *y* axis at *l*/*a*=0.0

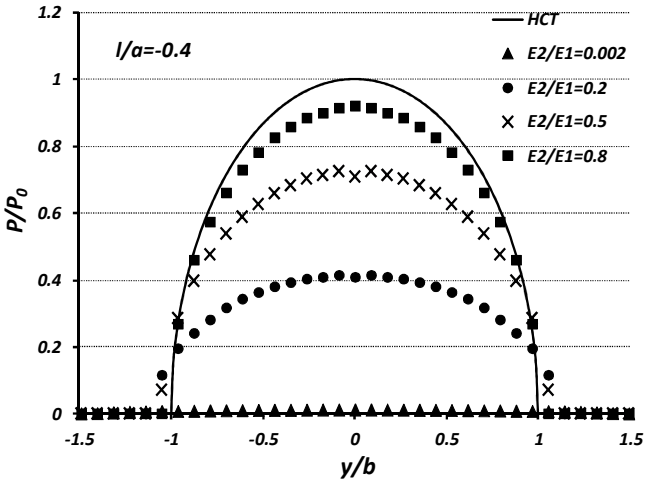

(b)

Fig. 11 Effect of various elastic modulus ratios on the contact pressure distribution along: (*a*) *x* axis; (*b*) *y* axis at *l*/*a*=-0.4

Fig. 10 (b) and Fig. 11 (b) illustrate the contact pressure along the *y* axis at contact distances l/a=0 and -0.4. Generally the pressure distribution keeps approximately an elliptical shape irrespective of E_2/E_1, and the magnitude decreases as the E_2/E_1 reduces. To further demonstrate the effect of the material modulus ratio on the contact pressure. Fig. 12 depicts three-dimensional contour plots of the contact stress for the cases of E_2/E_1=0.002 and 0.8. The presence of extreme low elastic stiffness for the insulation material i.e. E_2/E_1=0.002, will result in the loss of the contact and magnify the rail ends effect, while the insulation material with high elastic modulus, i.e. E_2/E_1=0.8 could provide more support to the wheel loading.

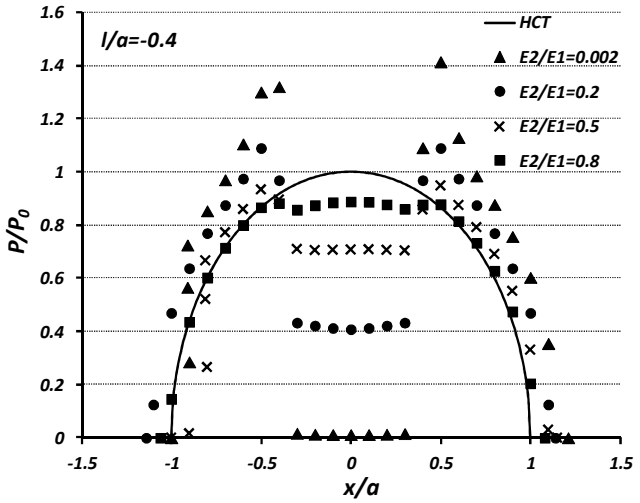

(a)

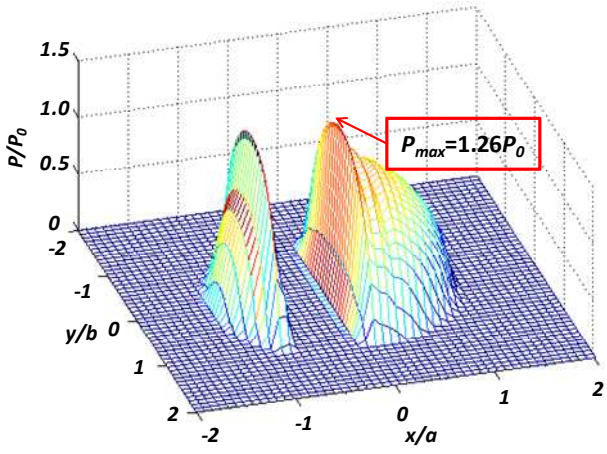

(a) E2/E1=0.002 at l/a=0.0

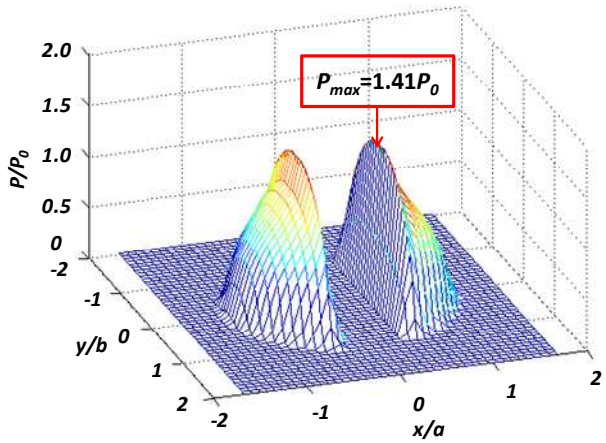

(b) E2/E1=0.002 at l/a=-0.4

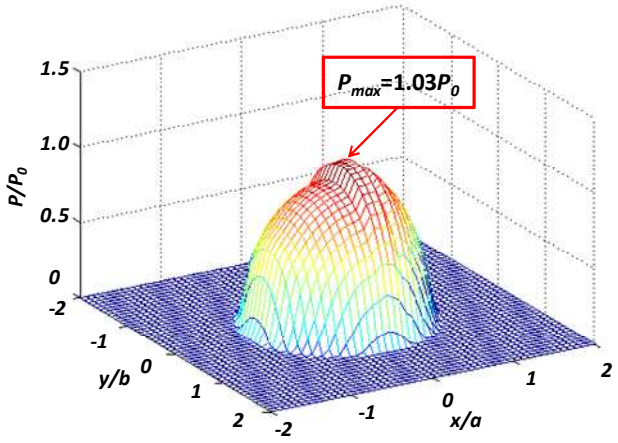

(c) E2/E1=0.8 at l/a=0.0

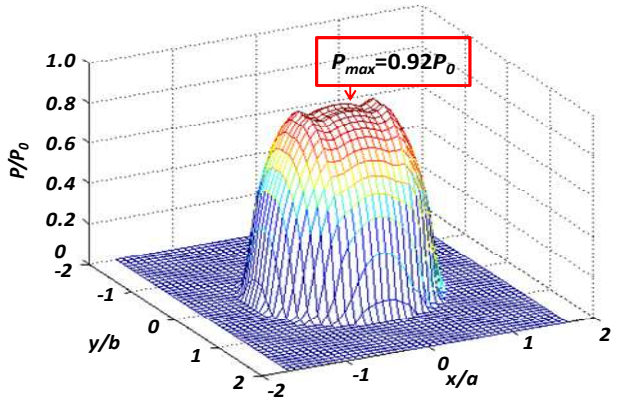

(d) E2/E1=0.8 at l/a=-0.4

Fig. 12 Three-dimensional contour plot of contact pressure distribution

Following the study of the effect of the elastic modulus ratio (E_2/E_1), the von Mises stress σ_e/P_0 and the shear stress τ_{max}/P_0 along the interface between the insulation material and the rail end are presented in Fig. 13 and Fig. 14 respectively. It is found that the magnitude of either the maximum shear stress or the von Mises stress will increase with the decreasing elastic modulus of insulation material, and they reach as high as $0.94P_0$ and $1.65P_0$ at l/a=0.0 and $1.13P_0$ and $2.0P_0$ at l/a=0.0 for E_2/E_1=0.002. The behaviour of such stresses reduction could be beneficial for slowing the process of delamination of the interface. However, further analysis in terms of the peak von Mises stress in the rail end and insulation material suggests that it is not always positive to increase the elastic modulus of the insulation material. As shown in Fig. 15, the difference of the maximum von Mises stress between the insulation material and the rail has been significantly reduced as E_2/E_1 changes from 0.002 to 0.8. As for E_2/E_1=1, the rail joint will act as the continuously welded rail (CWR) and the majority of the stress concentration zone will shift into the insulation material as predicted in Hertzian contact theory. This trend reveals although the higher ratio E_2/E_1 can slow down the interface delamination, the increasing stress level in the insulation material could lead to earlier damage or failure of insulation material, resulting the electrical failure of IRJ.

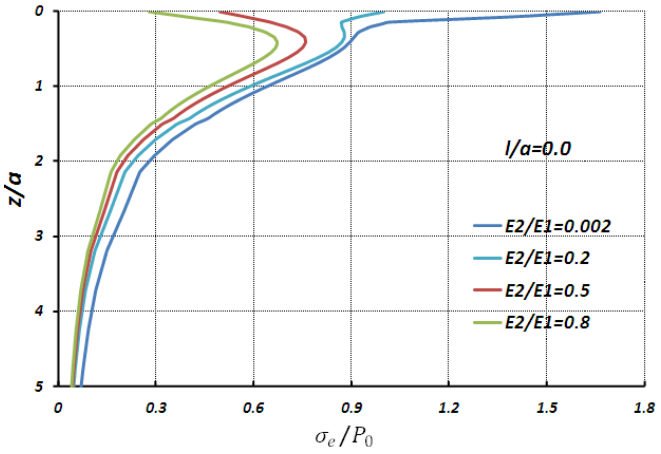

(a)

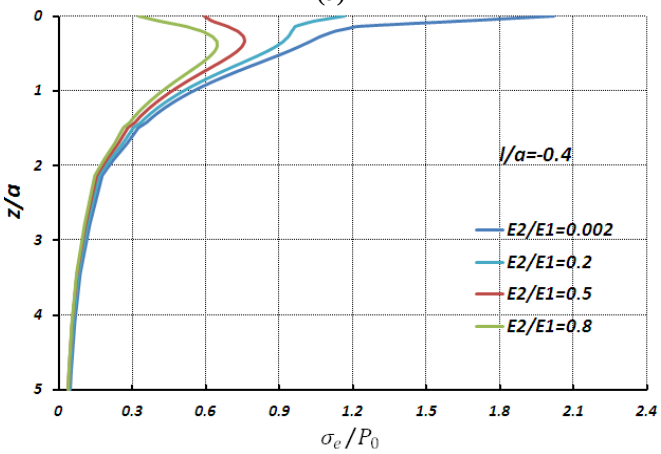

(b)

Fig. 13 Distribution of von Mises stress along the interface between rail end and insulation material at contact distance: (*a*) l/a=0.0; (b) l/a=-0.4

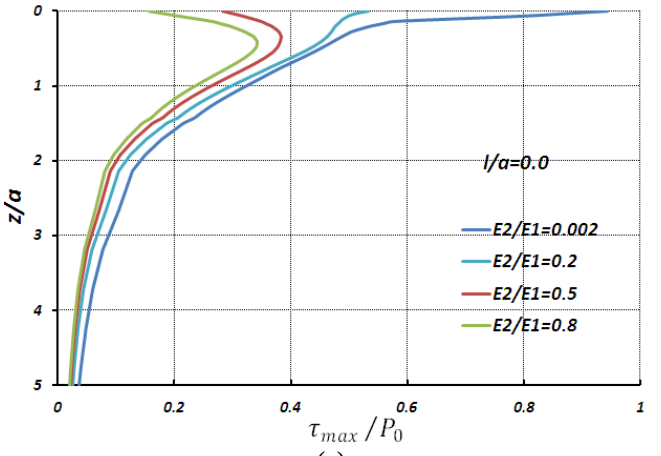

(a)

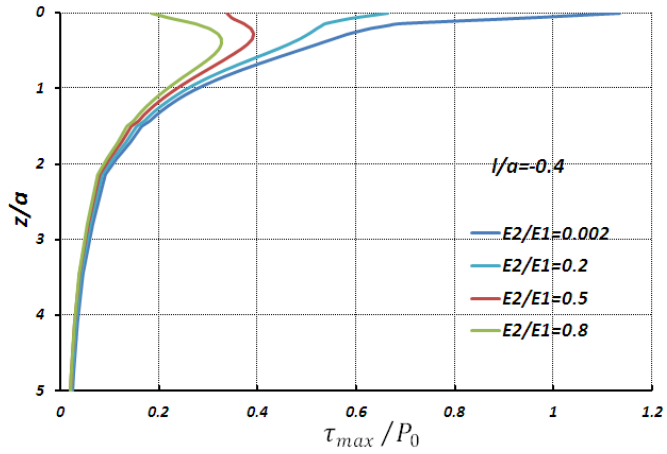

(b)

Fig. 14 Distribution of maximum shear stress along the interface between rail end and insulation material at contact distance: (*a*) *l/a*=0.0; (*b*) l/a=-0.4

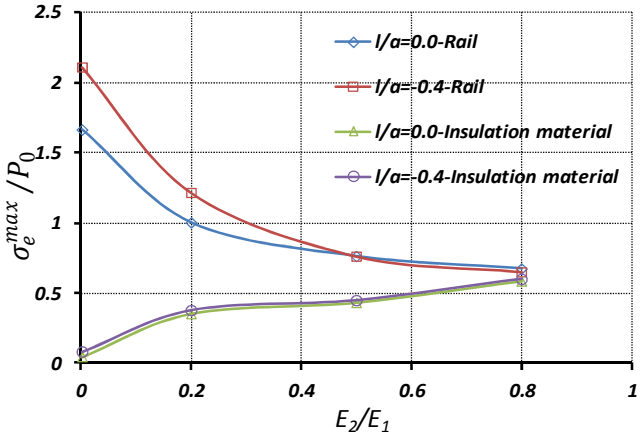

Fig. 15 Comparison of maximum von Mises stress in rail and insulation material at various ratios in elastic modulus

IV. Conclusions

The effects of material interface between rail end and insulation material to the wheel-rail contact in various proximities to the IRJ were investigated by using three-dimensional finite element model. Results based on FE analysis are presented and compared with relevant literature. Some conclusions are made as follows:

- Contact can be regarded as Hertzian when the wheel is at a distance l/a>0.96; beyond that Hertzian assumption is invalid;
- The response of the maximum shear stress and von Mises stress along the interface between the rail end and the insulation material was found to be quite sensitive to the contact positions of the wheel. As the wheel approaches the rail end, these stresses significantly increases;
- The stress concentration zone at rail end was also found to be amplified and its location migrates from the rail subsurface to the top surface as wheel moves to the rail end. This phenomenon can accelerate the railhead deterioration in the vicinity of gap end;
- The effect of the difference of elastic modulus between the insulation material and the rail was investigated. Results show that that a lower difference in elastic modulus can reduce the interface stress magnitude in the rail ends, however, it could adversely result in higher stress in the insulation material, which may lead to its earlier failure.

Acknowledgment

The authors are grateful to the CRC for Rail Innovation (established and supported under the Australian Government's Cooperative Research Centre program) for funding the research to the second author. Queensland University of Technology (QUT) provided fee waiver to the first author.

References

[1] Tan, X., and Bushan, B.: A numerical three-dimensional model for the contact of rough surfaces by variational principle. Journal of Tribology. 118: 33-42, 1996.
[2] Li, J., and Berger, E. J.: A Boussinesq-Cerruti solution set for constant and linear distribution of normal and tangential load over a triangular area. Journal of Elasticity. 63: 137-151, 2001.
[3] Wilner, K.: Fully coupled frictional contact using elastic halfspace theory. Journal of Tribology. 130: 031405, 2008.
[4] Chen, W. W., and Wang, Q. J.: A numerical static friction model for spherical contacts of rough surfaces, influence of load, material and roughness. Journal of Tribology. 131: 031405, 2009.
[5] Liu, S., and Hua, D. Y.: Three-dimensional semiperiodic line contact-periodic in contact length direction. Journal of Tribology. 131: 021408, 2009.
[6] Hetenyi, M.: A general solution for the elastic quarter space. Journal of Applied Mechanics, Transactions of the ASME. 39: 75–80, 1970.
[7] Keer, L. M., Lee, J. C., and Mura, T.: Hetenyi's elastic quarter space problem revised. International Jounal of Solids & Structures. 19: 497-508, 1983.
[8] Hanson, M.T., and Keer, L. M.: A simplifies analysis for an elastic quarter-space. Q. J. Mech. Appl. Math.. 43: 561-588, 1990.
[9] Guilbault, R., Gosselin, C. and Cloutier, L.: Express model for load sharing and stress analysis in helical gears. ASME Journal of Mechanical Design. 127: 1161-1172, 2005.
[10] Guilbault, R.: A fast correction for elastic quarter-space applied to 3D modeling of edge contact problems. Journal of Tribology. 133: 031402, 2011.
[11] Gerber, C. E.: Contact problems for the elastic quarter plane and the quarter space, Doctoral dissertation, Stanford University, CA, U.S.A, 1968.
[12] Erdogan, F. and Gupta, G.D.: Contact and crack problems for an elsatic wedge, International Journal of Engineering Science. 14: 155-164, 1976.
[13] Hanson, M .T., and Keer, L. M.: Stress analysis and contact problems for an elastic quarter-plane. Q. J. Mech. Appl. Math.. 42: 363-383, 1989.
[14] Keer, L.M., Lee, J.C. and Muta, T.: A contact problem for the elastic quarter space. International Journal of Solids & Structures. 20: 513-524, 1984.
[15] Bosakov, S.V.: Ritz's method in the contact problems of the theory of elasticity. Belarusian National Technical University (2007).
[16] Guenfoud, S., Bosakov, S.V. and Laefer, D.F.: A Ritz's method based solution for the contact problem of a deformable rectangular plate on an elastic quarter-space. Internatoinal Journal of Solids & Structures. 47: 1822-1829, 2010.
[17] Yan, W. and Fischer, F.D.: Applicability of the Hertz contact theory of rail-wheel contact problems. Archive of Applied Mechanics. 70: 255-268, 2000.
[18] Chen, Y.C.: The effect of proximity of a rail end in elastic-plastic contact between a wheel and a rail. Proceedings of the Institution of Mechanical Engineers, Part F: Journal of Rail and Rapid Transit. 217: 189–201, 2003.
[19] Chen, Y.C., and Kuang, J.H.: Contact stress variations near the insulated rail joints. Proceedings of the Institution of Mechanical Engineers, Part F: Journal of Rail and Rapid Transit. 216: 265-274, 2002.

[20] Wen, Z., Jin, X. and Zhang, W.: Contact-impact stress analysis of rail joint region using the dynamic finite element method. Wear. 258: 1301-1309, 2005.
[21] Cai, W., Wen, Z., Jin, X. and Zhai, W.: Dynamic stress analysis of rail joint with height difference defect using finite element method. Engineering Failure Analysis. 14: 1488-1499, 2007.
[22] Sandström, J., and A Ekberg, A.: Numerical study of the mechanical deterioration of insulated rail joints. Proceedings of the Institution of Mechanical Engineers, Part F: Journal of Rail and Rapid Transit. 223: 265–273, 2008.